PLOS ONE

RESEARCH ARTICLE

Optimizing information processing in neuronal networks beyond critical states

Mariana Sacrini Ayres Ferraz, Hiago Lucas Cardeal Melo-Silva, Alexandre Hiroaki Kihara*

Núcleo de Cognição e Sistemas Complexos, Centro de Matemática, Computação e Cognição, Universidade Federal do ABC, São Bernardo do Campo, SP, Brasil

* alexandrekihara@gmail.com

Citation: Ferraz MSA, Melo-Silva HLC, Kihara AH (2017) Optimizing information processing in neuronal networks beyond critical states. PLoS ONE 12(9): e0184367. https://doi.org/10.1371/journal.pone.0184367

Editor: Dante R. Chialvo, Consejo Nacional de Investigaciones Cientificas y Tecnicas, ARGENTINA

Received: May 29, 2017

Accepted: August 22, 2017

Published: September 18, 2017

Data Availability Statement: All relevant data are within the paper.

Funding: This research is supported by grant 2015/50122-0 from Sao Paulo Research Foundation (FAPESP) and DFG-IRTG 1740/2. HCM is grateful for UFABC scholarship. MAF is grateful for CNPq scholarship. AHK is grateful for grants from FAPESP (2014/16711-6) and CNPq (308608/2014-3). The funders had no role in study design, data collection and analysis, decision to publish, or preparation of the manuscript.

Abstract

Critical dynamics have been postulated as an ideal regime for neuronal networks in the brain, considering optimal dynamic range and information processing. Herein, we focused on how information entropy encoded in spatiotemporal activity patterns may vary in critical networks. We employed branching process based models to investigate how entropy can be embedded in spatiotemporal patterns. We determined that the information capacity of critical networks may vary depending on the manipulation of microscopic parameters. Specifically, the mean number of connections governed the number of spatiotemporal patterns in the networks. These findings are compatible with those of the real neuronal networks observed in specific brain circuitries, where critical behavior is necessary for the optimal dynamic range response but the uncertainty provided by high entropy as coded by spatiotemporal patterns is not required. With this, we were able to reveal that information processing can be optimized in neuronal networks beyond critical states.

Introduction

Maximum unpredictability is reported to occur around phase transitions where criticality is observed. This hypothesis finds important concrete realizations in biological systems, including the brain physiology [1]. Although it is still under discussion, a cornerstone from the theoretical perspective is that neuronal networks work in the vicinities of a critical regime, i.e., the activities observed in the neuronal networks, *in vivo* [2,3,4,5], *in vitro* [2,6,7,8,9,10] *silico* [1,11,12,13], are found to exhibit neuronal-avalanche-like behaviors whose size distribution can be approximated by a power law.

The critical regime is known to provide some advantages for processing in network systems. In the neuronal network context, we can cite the maximization of both information processing [2,3,11] and dynamic range [1,11]. Information processing in the brain has been studied through interdisciplinary perspectives, including biological, psychophysical, and mathematical approaches [1,2,8,14,15,16]. As a theoretical example, a network of excitable elements maximizes information processing at the critical point compared with that at other conditions such as sub- and super-critical regimes [1]. The enhancement of dynamic range particularly favors neuronal networks in sensory systems [1,7]. This

Competing interests: The authors have declared that no competing interests exist.

finding is compatible with the role of connexin-mediated communication in electrical synapses observed in the retina [17,18,19,20] and olfactory glomeruli [21,22].

Different regions of the brain, other than the sensory systems, have diverse functionalities and their activity patterns are responsible for coding and storing information. Experiments have shown that information in the cortex and hippocampus are provided through repeated spatiotemporal patterns [6,23,24,25,26,27,28] that are related to memory consolidation [24,28]. Thus, neuronal avalanches present themselves as highly diverse and also repeatable [6].

Although the pattern variability in criticality is maximum [11,13], the manner in which these patterns occur in critical networks and the way they are related to the micro-parameters of the network has not been explored thoroughly. In this study, we investigated the process of encoding information by a neuronal network in the critical regime. Furthermore, we employed simple branching process based models to demonstrate the distinct information capacity displayed by the critical networks. Our findings are compatible with those of the distinct neuronal circuitries observed in the brain, in which different information capacities are required while preserving the dynamical range provided by the critical state.

Methods

Network construction and avalanche statistics

The model used here is based on that reported previously [1]. Despite its simplicity, considering only excitatory probabilistic neurons, it is highly suitable for our goals. Briefly, the network has N excitable elements, where each element, i, has n states: $s_i = 0$ is the resting state, $s_i = 1$ is the excited state, and the remaining states, $s_i = 2,3,\ldots,n-1$, are refractory states. The ith element can reach the state $s_i = 1$ from $s_i = 0$ in two different ways; (1) because of an external stimulus provided by a Poisson process with rate r (transition probability $\lambda = 1-\exp(-r\Delta t)$ per time step, $\Delta t = 1$ ms), or (2) with probability p_{ij} because of a neighbor j being in the state $s_j = 1$ in the previous time step. The dynamics after excitation are deterministic, i.e., after $s_i = 1$, in the next step it will change to $s_i = 2$, and this will continue to occur until state $s_i = n-1$ leads to the $s_i = 0$ resting state, forming a cyclic cellular automaton. We employed an Erdös–Rényi undirected random network, with $NK/2$ links assigned to randomly chosen pairs of elements. Therefore, we obtain a network with average connectivity K, where each element $i = 1,2,\ldots,N$ is randomly connected to K_i neighbors. The probability p_{ij} of an element j activates another element i is given by a random variable with uniform distribution in the interval $[0,p_{\max}]$. The local branching ratio is given by $\sigma_j = \sum_i^{K_j} p_{ij}$ and corresponds to the average number of excitations generated in the next time step by the jth element. The average branching ratio $\sigma = \langle \sigma_i \rangle$ is the parameter that sets the criticality ($\sigma = 1$), which is chosen using $p_{\max} = 2\sigma/K$.

The average activity F is defined as $F = T^{-1}\sum_{t=1}^{T}\rho_t$, where ρ_t is the network instantaneous density activity of elements $s = 1$ at time t and T is a large time window (of the order of 10^3 ms) [1]. The response curve is defined as the average activity, F, dependent on the stimulus rate r. The network has a minimum response, F_0, and a maximum response, $F_{\max}$. The dynamic range is defined as $\Delta = 10\log\left({}^{r_{0.9}}/_{r_{0.1}}\right)$, in dB, as the interval whose variations in the stimulus result in robust variations of F. The interval $[r_{0.1}, r_{0.9}]$ is found from the correspondent interval $[F_{0.1}, F_{0.9}]$, where $F_x = F_0 + x(F_{\max}-F_0)$ [1].

The avalanches were triggered by the random activation of one single element and the spontaneous activity was recorded till the active elements became absent. The avalanche size was defined as the amount of involved active elements without considering repetitions. This procedure was repeated n_{ava} times to generate the probability density function (PDF) of

avalanche sizes. We also calculated the linear least squares regression to check the power law exponent and the R-squared coefficient.

Spatiotemporal activity entropy evaluation

To evaluate the entropy on the basis of the activity of the networks, 10% of the elements were randomly activated at the initial time. First, as an indication of the homogeneity of individual element activity during n_{ava} avalanches, we counted the number of times each element was activated ($s = 1$). Thus, we were able to obtain the activation PDF of element i, $F_S(i)$. If the activity between the elements was homogeneously distributed, a flat distribution would have been observed. Therefore, we used a theoretical curve of a constant PDF $F_C(i)$ as reference. We defined the parameter Δd as a measure of the distance between the PDF obtained by simulation in relation to the theoretical one:

$$\Delta d = \frac{1}{N}\sum_{i=1}^{N}|F_C(i) - F_S(i)|.$$

The greater the value of Δd was, lesser was the homogeneity of the resulting activity.

In order to calculate the activity entropy, we reduced the random networks to full connected smaller ones of size N'. The reduction was obtained by following these steps, as shown in Fig 1B: (i) n_{ava} avalanches were simulated with the time window T^j_{ava} (explained later), with $j = 1,2,\ldots,n_{ava}$; (ii) the elements of the networks were set in an order in a matrix of $N \times T^j_{ava}$ for each avalanche on the basis of their activity; (iii) the dimension of the matrix was reduced by a factor c, where $N' = N/c$, thereby grouping sequential elements; (iv) each new element was considered active if n_{act} amount of its components were activated; (v) the probability of activation of each element with time, $p^i_a t$, was calculated for each new element, with $i = 1,2,\ldots,N$; (vi) the mean probability by avalanche $\langle p^i_a t\rangle_{n_{ava}}$ was calculated. The time window T^j_{ava} of the jth avalanche was shown in Fig 1A. It was defined as the interval that corresponded to the period

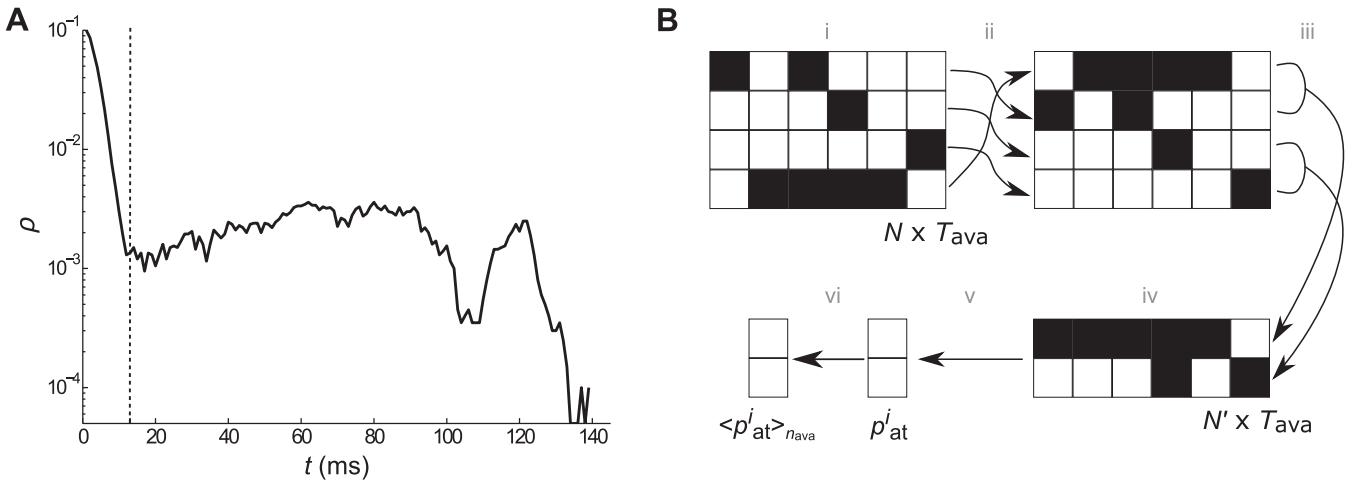

Fig 1. Reduction method employed in the analysis of the network activity. Method used to obtain a smaller network, which resembled the same features of activation probability density function F_S as those of the original. (A) Example of the network density activity ρ during the jth avalanche. The time window T^j_{ava} starts at approximately 13 ms. (B) Simplified representation of the reduction method. The first step was the arrangement of the element activities during an avalanche in a matrix of size $N \times T^j_{ava}$ (step i), followed by ordering the elements according to their activity (step ii). The dimension of the matrix was reduced by a factor of $c = 1250$, grouping sequential elements (step iii), and each new element was considered active if at least 2 of its components was activated (step iv). Then, the probability of activation of each element was calculated by time, $p^i_a t$ (step v), and finally the mean from $n_{ava} = 10\,000$ avalanches, $\langle p^i_a t\rangle_{n_{ava}}$, was calculated (step vi).

https://doi.org/10.1371/journal.pone.0184367.g001

after the initial high activity provoked by the external stimulus and after the final drop. T_{ava} was the longest of all T^j_{ava}, i.e., $T_{ava} = \max\{T^j_{ava} | j = 1, 2, \ldots, n_{ava}\}$.

After determining $\langle p^i_a t \rangle_{n_{ava}}$ for each element i, we applied a minimalistic model for the network dynamic. In this model, the elements had two states, active and inactive, indicated by 1 and 0, respectively. The model started with one randomly chosen single active element. For each step, the active nodes in the previous step became 0 and remain 0 for one more time step, the nodes i that had active neighbours j in the previous step have the probability p'_{ji} to become active.

In order to obtain the news p'_{ij} for the reduced networks, we normalized $\langle p^i_a t \rangle_{n_{ava}}$ by its mean value and obtained one variable similar to the σ_i, defined as γ_i. So, the $p'_{ji} = \frac{\gamma_i}{N'}$, with $p'_{ij} \neq p'_{ji}$ and $\gamma_i = \sum_{j=1}^{N'} p'_{ji}$. While σ_i is related to the number of activation that departs from element i, λ_i is related to the number of possible neighbours that are able to activate the element i.

The activity entropy H_A was based on the spatiotemporal patterns of the avalanches. For each time step, we represented the activity by a vector of size $1 \times N'$. An avalanche of length t' was created by concatenating t' vectors into a single one of size $1 \times N't'$ [2]. These vectors were then tested using a similarity matrix. For the original networks the length t' was chosen by setting $t' = T_{ava}$, and for the reduced networks we considered the same time window for all the avalanches. We did not take into account the initial time, and by doing this we did not consider the first random active element in each avalanche.

The similarity between two patterns varied from 0 to 1, and is defined as [11]:

$$\mathrm{Sim}\left(v_i, v_j\right) = \frac{\langle v_i, v_j \rangle}{\langle v_i, v_i \rangle + \langle v_j, v_j \rangle - \langle v_i, v_j \rangle},$$

where $\langle \cdot, \cdot \rangle$ is a dot product and v are the vectors of configurations. Finally, the entropy H_A, in bits, was defined as $H_A = -\sum_i p_i \log_2(p_i)$, where p_i is the probability of the ith activity configuration considering the total patterns found when Sim $\geq th$, with th is an arbitrary threshold.

Results

Networks with different connectivities produce similar dynamic features

We started simulating avalanches in critical networks using the methodology described before. We generated networks with the same number of nodes but distinct mean connectivities K. The simulations were performed using 3 chosen values of K, $K = 10$, 100, and 1 000, with $N = 20\,000$. Fig 2A and 2B show the K_i and branching parameter σ_i distributions for the three cases. The K_i distributions were centralized in 0, that is, $K_i - K$. Because the inverse dependence between the p_{max} and K parameters, as the $P(K_i)$ became more broad, the $P(\sigma_i)$ became more sharp. We used σ as the control parameter because of the randomness of the p_{ij}. Otherwise, it is known that the best parameter control is given by the largest eigenvalue of the connection matrix [29].

Fig 2C show the avalanche size distributions calculated for $n_{ava} = 10\,000$, where the dashed line is a curve with a referent slope of −1.5. The slopes were calculated using linear least squares regression, which provided the fitted exponent values of −1.48 (−1.55, −1.41), −1.47 (−1.54, −1.41), and −1.45 (−1.52, −1.39) for $K = 10$, 100, and 1 000, respectively, with R-square value of 0.99 for all fits. The dynamic range responses related to σ were also calculated (Fig 2D) showing similar values for all networks. Although the networks have different K and distributions of K_i and σ_i, all three exhibited very similar avalanche statistics as revealed by the power law fitting, including similar dynamic responses.

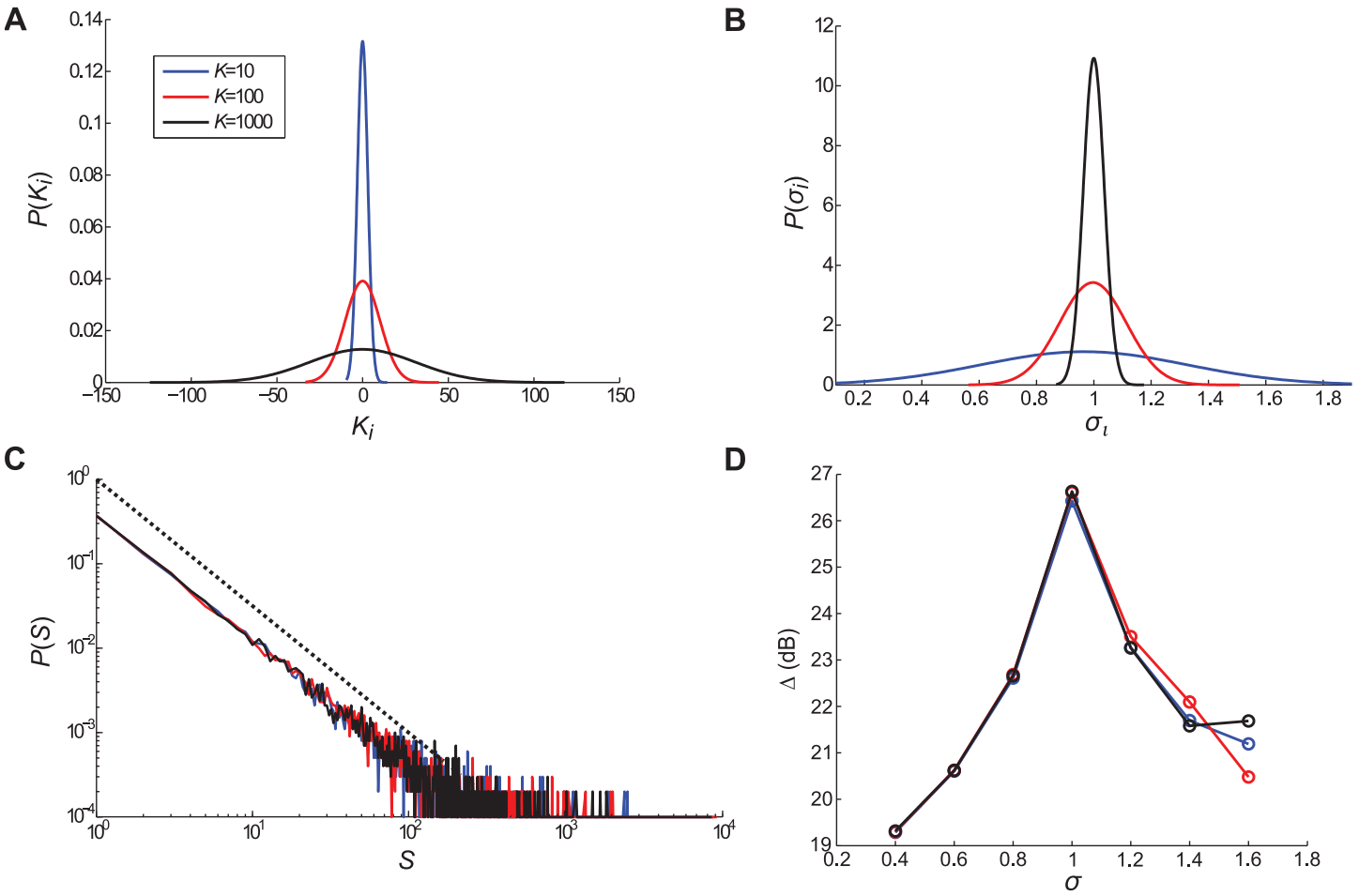

Fig 2. General features of the networks and activity. In our network model, the total number of elements was $N = 20\,000$ and we used 3 distinct values for mean connectivity; $K = 10$, 100, and 1 000. We simulated $n_{ava} = 10\,000$ avalanches triggered by one random active element in the initial time with a dynamic model based on [1], as explained in the Methods section. (A) Probability density distributions of connectives K_i $P(K_i)$ for $K = 10$ (red), 100 (blue), and 1 000 (black) centralized in 0, that is, K_i–K. (B) Probability density distributions of the branching parameters σ_i $P(\sigma_i)$ for $K = 10$ (red), 100 (blue), and 1 000 (black). (C) Probability density distributions of the avalanche sizes $P(S)$ for $K = 10$ (red), 100 (blue), and 1 000 (black). The dashed black line has a reference slope of −1.5. (D) Dynamic range Δ *versus* σ for networks with $K = 10$ (red), 100 (blue), and 1 000 (black).

https://doi.org/10.1371/journal.pone.0184367.g002

Homogeneity of activity in network elements depends on mean connectivity

As we were able to determine that networks with distinct mean connectivities produce similar global dynamics, we next investigated the individual activity during the avalanches. Therefore, we analysed the activation PDF, F_S, of the element i and the homogeneity index, Δd, for the above-mentioned 3 cases with $n_{ava} = 10\,000$, $N = 20\,000$, and 10% of active initial elements (Fig 3). Fig 3A shows F_S for $K = 10$, 100 and, 1 000, with F_C as the homogeneity reference. The overlapped lines represent results from 10 networks of each case. Fig 3B shows the results of mean, Δd, and the errors obtained, i.e., $(16.300 \pm 0.060) \cdot 10^{-6}$, $(7.400 \pm 0.014) \cdot 10^{-6}$, and $(6.150 \pm 0.005) \cdot 10^{-6}$ for $K = 10$, 100, and 1 000, respectively. Our simulations revealed that homogeneity of activity in network elements depended on the mean connectivity. Indeed, higher values of K resulted in smaller Δd values. As shown in Fig 2A and 2B, smaller K implies a broad σ_i distribution, leading to a higher variety of σ_i values. The largest values could produce more probably paths, in contrast to the smallest ones. That way, these results revealed that

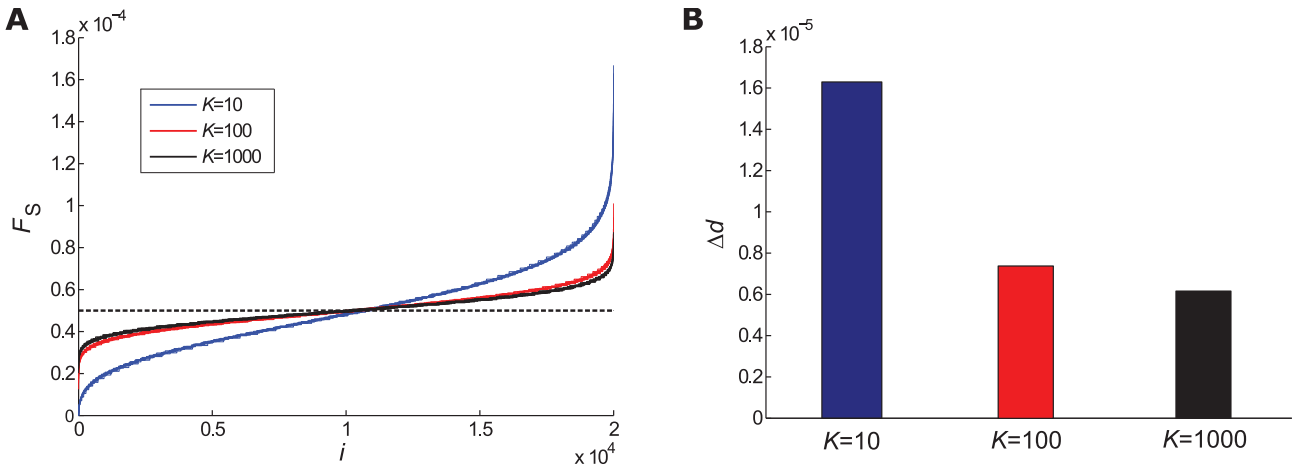

Fig 3. Analysis of individual element activity. The activity of each element *i* of the networks during the avalanches was computed and activation probability density function (PDF) of elements *i* F_S was calculated. We simulated n_{ava} = 10 000 triggered by random 10% active initial elements. (A) We simulated activity in 10 distinct networks for each mean connectivity, K = 10 (red), 100 (blue) and 1 000 (black). The dashed black line represents homogeneity reference PDF, F_C. All 10 simulations were plotted in the graph and appeared as overlapped lines. (B) We also calculated the mean difference Δd index between the results obtained for each condition and those obtained for the reference line.

https://doi.org/10.1371/journal.pone.0184367.g003

homogeneity in the involvement of individual elements in the network activity varied depending on the mean connectivity, although the global features were very similar.

Network reduction method maintains similar activation features of the original networks

Networks made up with different configurations, although had showed similar avalanches features and dynamic responses, could hidden features that could only be seen if one had looked closer. In order to analyse the spatiotemporal patterns of the activity in these networks with more details, we employed a reduction method. The reduction decreased the number of possible paths facilitating the analyses, besides ensures the same features of F_S as those of the original simulated networks. Moreover, in reduced networks we were able to maintain the same K, as $K = N' - 1 = 15$. (Fig 1). First, we chose the time window T^j_{ava} as the interval corresponding to the period after the initial high activity provoked by the external stimulus and after the final drop (Fig 1A). In our analysis we computed spatiotemporal patterns after 13 ms to avoid the background activity related to the random stimulus and T_{ava} = 413,462, and 273 ms for K = 10, 100, and 1 000, respectively. We then arranged the avalanche into a matrix of size $N \times T^j_{ava}$ (step i) and ordered it by activity (step ii). The dimension of the matrix was reduced by a factor of c = 1 250, grouping sequential elements (step iii). Each new element was considered active if at least n_{act} = 2 of its components was activated (step iv) (Fig 1B). Then, we computed the probability of activation of each element with time $p^i_a t$ (step v) and finally the mean from n_{ava} = 10 000 avalanches $\langle p^i_a t \rangle_{n_{ava}}$ (step vi). The values obtained for $\langle p^i_a t \rangle_{n_{ava}}$ are shown in Fig 4A. These probabilities were used in the reduced networks, as explained in the next section. It is noted that the curves collapsed themselves when the transform $(\langle p^i_a t \rangle_{n_{ava}} - 0.5)(K)^{1/2}$ is used. Results were shown as inset in Fig 4A. We observed that the same dependence with K was valid for the F_S.

There is a little difference between calculation of F_S and $\langle p^i_a t \rangle_{n_{ava}}$, but they follow the same general tendency as we can see for the original network with K = 10 as example (Fig 4B). That

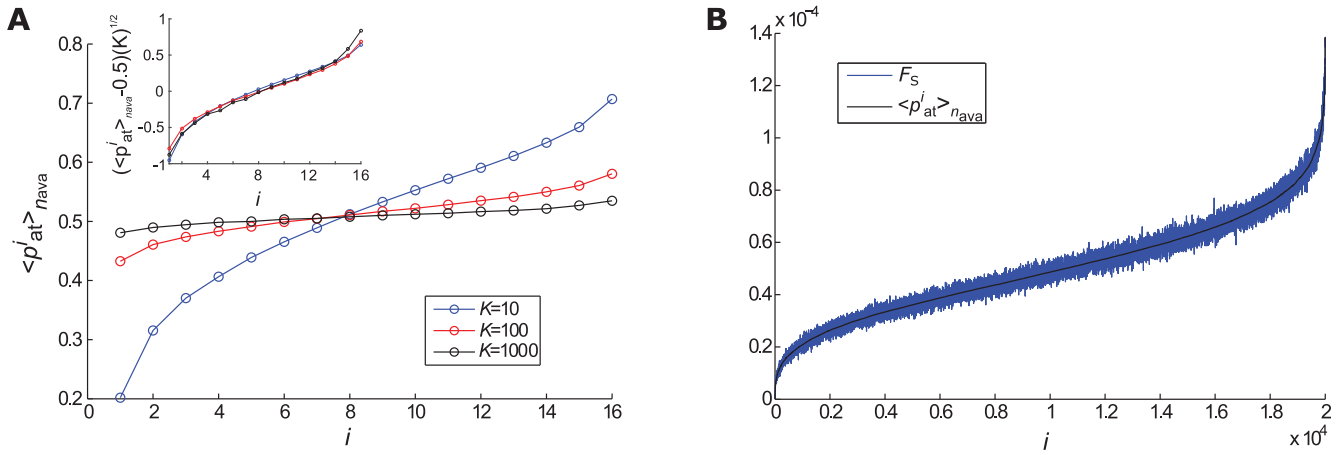

Fig 4. The probability of activation of the reduced networks *versus* the original networks. The reduction methods generated the activation probability for the reduced networks, and keep the tendency with the F_S. (A) The activation probabilities $\langle p_a^i t \rangle_{n_{ava}}$ of the reduced networks for the three cases, $K = 10$ (red), 100 (blue) and 1 000 (black). The inset shows the collapsed curves adopting $(\langle p_a^i t \rangle_{n_{ava}} - 0.5)(K)^{1/2}$. (B) Example of the tendency between the $\langle p_a^i t \rangle_{n_{ava}}$ and the F_S for the original network with $K = 10$. Both were normalized by the area under the curve.

https://doi.org/10.1371/journal.pone.0184367.g004

way, the F_S of the simulations of the reduced networks could be calculated to check the method functionality.

Entropy as coded by spatiotemporal patterns depends on mean connectivity

The capacity of a network stores information is related to the nodes that are activated, for example, in a neuronal network. Not only the amount of nodes, but the temporal sequence of activation, and if the same sequence could be posteriorly achieved again. A highly used way to characterize the distribution of these patterns is based on the Shannon entropy, and can give us some clues of how the entropy can vary in critical networks.

To evaluate the entropy based on spatiotemporal patterns we used the reduced-sized networks for our simulations from now on. Then, each one of the original networks generated a reduced one, which are shown in Fig 5A, 5B and 5C. They are fully connected and the nodes activation probability are featured by the colour distribution. For the simulations we chose $N' = 16$, $t' = 4$ ms and $n_{ava} = 10\,000$. Calculating the F_S, the results are shown in Fig 5D, from which we can see the agreement between the values obtained from reduced and original networks, both normalized by the area under the curve.

The simulated avalanches generated 10 000 vectors of activity of size $1 \times N't'$. Based on these vectors, we calculated the similarity matrix. Applying the threshold $Th = 0.7$, all values above it were considerated as 1 and below it as 0. That way, we identified all similar patterns and computed the activity entropy H_A. Fig 5E shows one example for $K = 10$ related to patterns that repeated more frequently (top), as well as patterns that repeated less frequently (bottom). We can see that the less repeated patterns were generally composed by the elements with low activation probability, in contrast with the more repeated patterns. The vertical line separates the initial time, when the active element was chosen randomly. Fig 6A shows that maximum repeatability of the patterns and Fig 6B the H_A *versus* the deviation of the σ_i distribution. The markers colour are related to the referent K and the colourless marker are the theoretical value idealized for a network with 10 000 avalanches and 0 patterns repeated. We can see that the

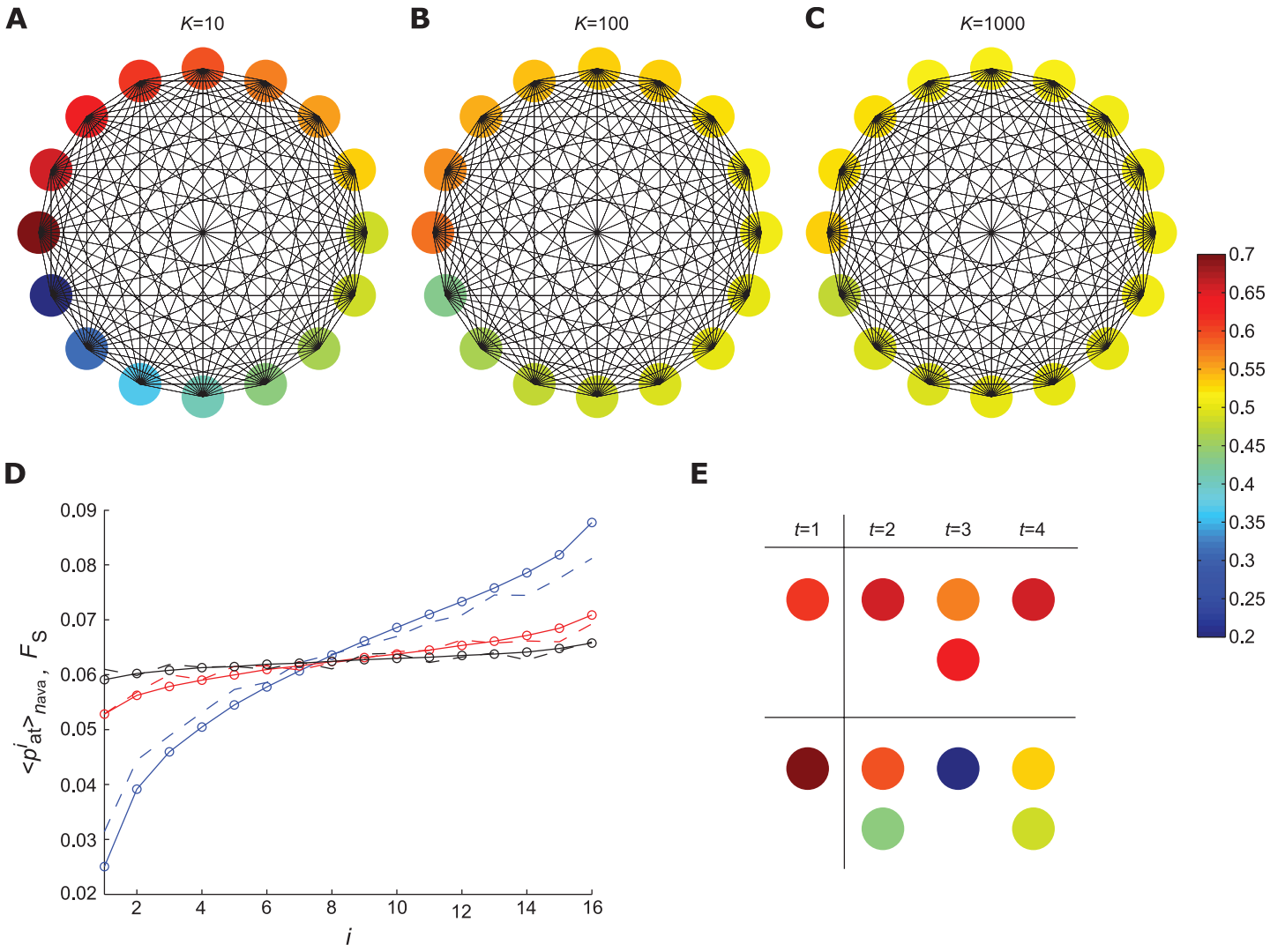

Fig 5. Reduced networks. Scheme of the $\langle p_a^i t \rangle_{n_{ava}}$ for the reduced networks. (A), (B) and (C) show the activation probabilities $\langle p_a^i t \rangle_{n_{ava}}$ coming from the original three cases, $K = 10$, 100 and 1 000 respectively, distributed in fully connected reduced networks of size $N = 16$. (D) show the comparison between $\langle p_a^i t \rangle_{n_{ava}}$ obtained from the original networks, circles, and the F_S calculated from the simulations of the reduced networks, dashed lines, both normalized by the area under the curve. The colours blue, red and black are related to $K = 10$, 100 and 1 000 respectively. (E) Example of patterns observed in networks with $K = 10$. The pattern that was observed more frequently is located in the top, whereas the pattern that was observed less frequently is located in the bottom. The vertical line separates the initial time, when the active element was chosen randomly.

https://doi.org/10.1371/journal.pone.0184367.g005

repeatability increases as the deviation increases (or the K decreases) and the H_A has the opposite behaviour.

We were able to determine that the entropy increased monotonically with K, reinforcing the results observed in Fig 3. Indeed, the most likely spatiotemporal patterns increased the probability of repetition and decreased the entropy. In contrast, an increase in K produced more equi-probable spatiotemporal patterns, leading to an increase in entropy.

Discussion

Critical dynamics have been considered as an optimum regime for neuronal networks, mainly to enhance both information processing and dynamic range. Despite the importance of the

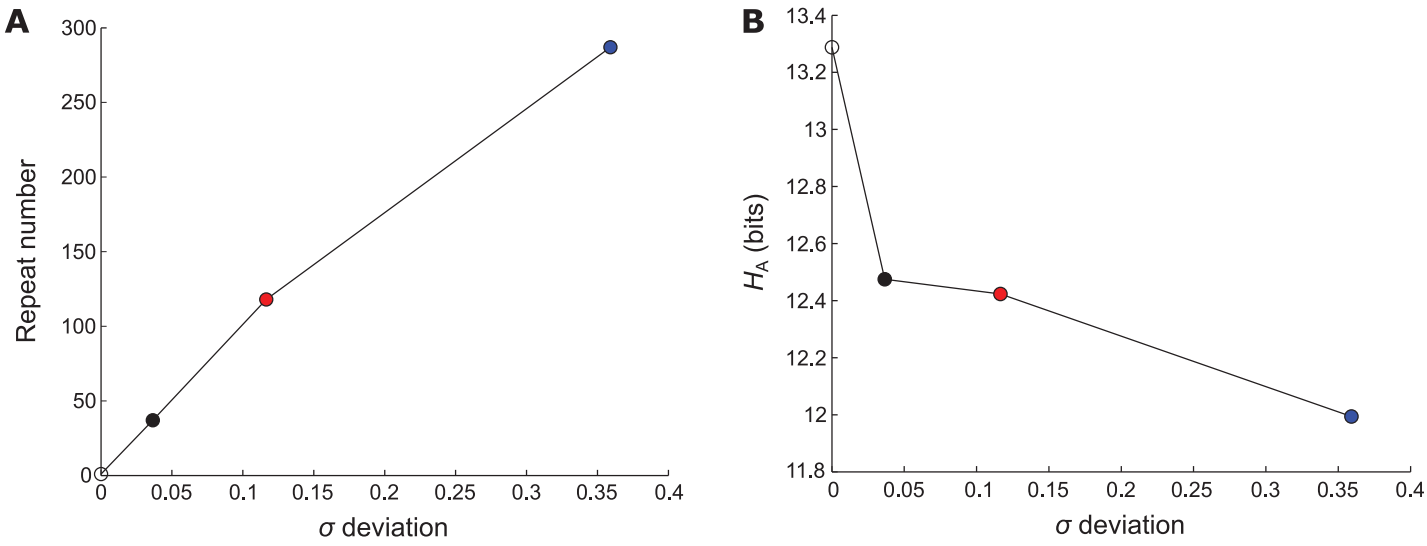

Fig 6. Analyses of the entropy as the result of spatiotemporal patterns. A minimalistic model was applied for the dynamics in the reduced networks with size $N' = 16$, activation probabilities $\langle p_a^i t \rangle_{n_{ava}}$, $n_{ava} = 10\,000$ and $t' = 5$ ms, as described in Methods section. The avalanches were compared using similarity matrix, and were subjected to an arbitrary threshold $th = 0.7$ in order to identify the similar patterns. The initial activated elements were not take into account. After this, we identified the number of different patterns and the maximum repeatability founded in each case. (A) The maximum repeatability of each case *versus* the σ_i deviation. (B) The entropy H_A *versus* the σ_i deviation. The associated K with the σ_i deviation is colour highlighted. Blue, red and black are related to $K = 10$, 100 and 1 000 respectively. The colourless circle is associated to the theoretical result where repetition is not observed.

https://doi.org/10.1371/journal.pone.0184367.g006

criticality, the knowledge about embedding information in the phase transition provided by this regime is very limited.

In this study, we employed branching process based models to study the spatiotemporal activity entropy. Our results revealed that the information capacity of networks set within the limits of critical dynamics may vary depending on the choice of parameters. Distinct values of K resulted in different distributions of σ with equal means but decreasing standard deviations. A large deviation in σ led the networks to superimpose some paths that repeated more than others, even creating a large number of patterns such as those fitted to a power law distribution.

The existence of more likely paths induced a reduction in the entropy as coded by spatiotemporal patterns. Therefore, it was possible to obtain variations in the information capacity even inside the critical regime, which does not interfere with both input sensitivity and dynamic response range. Moreover, adaptation in dynamic range response has been investigated as a physiological mechanism in neuronal cortical networks [30].

Although the model employed here has specific features, such as the dependence of K and σ variables, our results can be extended to neuronal biology. In this context, the synaptic plasticity plays a fundamental role, increasing or decreasing the recurrence of certain connections, producing more or less likely spatiotemporal activity paths. We can speculate that this balance is required in a neuronal network. For example, in circuitries related to memory and learning, spatiotemporal patterns may repeat more frequently than expected by chance. In this condition, neuronal circuitries do not work in full capacity in relation to the information, although this particular feature is maximum in critical regime.

Others models have been used to examine the repetitive patterns found in neuronal activities, such as the spike-timing dependent plasticity (STDP)-based learning process [13,31], where phase coded spike patterns are stored in the synaptic connections. Another example is related to learning model presented by de Arcangelis *et al.* [32]. In that paper the authors

showed a network model with plastic synaptic strength that presented critical behaviour and also was able to learn. They concluded that the system learns more efficiently as more possible spatiotemporal paths exist. However, in a simpler version, branching process models can achieve repeatable patterns, more or less, changing the deviation of the branching parameter, which may also result in controlling of information capacity.

To summarize, our findings disclosed new theoretical predictions involving dynamics and topology in real neuronal networks. For example, it was possible to postulate that brain circuitries located in the cortex might comprise a large amount of information as encoded by numerous distinct spatiotemporal patterns [6]. In contrast, we demonstrated that other circuitries may show a dynamic response, but with less information entropy. For example, when compared with those of the cortex, neuronal circuitries in the brain stem might not require a massive combination of distinct spatiotemporal patterns, although circuitries should be able to maintain optimum sensitivity to stimulus. Notably, a large variety of neuronal subtypes in the brain stem have been described [33,34]. The role of morphological heterogeneity, which may underlie variations in the connectivity degree, in the formation of networks with decreased entropy is a matter that needs to be empirically investigated.

Author Contributions

Conceptualization: Mariana Sacrini Ayres Ferraz, Hiago Lucas Cardeal Melo-Silva, Alexandre Hiroaki Kihara.

Data curation: Mariana Sacrini Ayres Ferraz, Hiago Lucas Cardeal Melo-Silva, Alexandre Hiroaki Kihara.

Formal analysis: Mariana Sacrini Ayres Ferraz, Hiago Lucas Cardeal Melo-Silva.

Investigation: Hiago Lucas Cardeal Melo-Silva, Alexandre Hiroaki Kihara.

Methodology: Mariana Sacrini Ayres Ferraz, Hiago Lucas Cardeal Melo-Silva, Alexandre Hiroaki Kihara.

Project administration: Alexandre Hiroaki Kihara.

Resources: Alexandre Hiroaki Kihara.

Supervision: Alexandre Hiroaki Kihara.

Validation: Mariana Sacrini Ayres Ferraz, Hiago Lucas Cardeal Melo-Silva.

Visualization: Mariana Sacrini Ayres Ferraz, Hiago Lucas Cardeal Melo-Silva, Alexandre Hiroaki Kihara.

Writing – original draft: Mariana Sacrini Ayres Ferraz, Hiago Lucas Cardeal Melo-Silva, Alexandre Hiroaki Kihara.

Writing – review & editing: Mariana Sacrini Ayres Ferraz, Alexandre Hiroaki Kihara.

References

1. Kinouchi O, Copelli M (2006) Optimal dynamical range of excitable networks at criticality. Nature Physics 2: 348–352.
2. Shew WL, Yang H, Yu S, Roy R, Plenz D (2011) Information capacity and transmission are maximized in balanced cortical networks with neuronal avalanches. J Neurosci 31: 55–63. https://doi.org/10.1523/JNEUROSCI.4637-10.2011 PMID: 21209189
3. Beggs JM, Plenz D (2003) Neuronal avalanches in neocortical circuits. J Neurosci 23: 11167–11177. PMID: 14657176

4. Petermann T, Thiagarajan TC, Lebedev MA, Nicolelis MA, Chialvo DR, et al. (2009) Spontaneous cortical activity in awake monkeys composed of neuronal avalanches. Proc Natl Acad Sci U S A 106: 15921–15926. https://doi.org/10.1073/pnas.0904089106 PMID: 19717463
5. Gireesh ED, Plenz D (2008) Neuronal avalanches organize as nested theta- and beta/gamma-oscillations during development of cortical layer 2/3. Proc Natl Acad Sci U S A 105: 7576–7581. https://doi.org/10.1073/pnas.0800537105 PMID: 18499802
6. Beggs JM, Plenz D (2004) Neuronal avalanches are diverse and precise activity patterns that are stable for many hours in cortical slice cultures. J Neurosci 24: 5216–5229. https://doi.org/10.1523/JNEUROSCI.0540-04.2004 PMID: 15175392
7. Shew WL, Yang H, Petermann T, Roy R, Plenz D (2009) Neuronal avalanches imply maximum dynamic range in cortical networks at criticality. J Neurosci 29: 15595–15600. https://doi.org/10.1523/JNEUROSCI.3864-09.2009 PMID: 20007483
8. Pasquale V, Massobrio P, Bologna LL, Chiappalone M, Martinoia S (2008) Self-organization and neuronal avalanches in networks of dissociated cortical neurons. Neuroscience 153: 1354–1369. https://doi.org/10.1016/j.neuroscience.2008.03.050 PMID: 18448256
9. Plenz D, Thiagarajan TC (2007) The organizing principles of neuronal avalanches: cell assemblies in the cortex? Trends Neurosci 30: 101–110. https://doi.org/10.1016/j.tins.2007.01.005 PMID: 17275102
10. Tetzlaff C, Okujeni S, Egert U, Worgotter F, Butz M (2010) Self-organized criticality in developing neuronal networks. PLoS Comput Biol 6: e1001013. https://doi.org/10.1371/journal.pcbi.1001013 PMID: 21152008
11. Haldeman C, Beggs JM (2005) Critical branching captures activity in living neural networks and maximizes the number of metastable States. Phys Rev Lett 94: 058101. https://doi.org/10.1103/PhysRevLett.94.058101 PMID: 15783702
12. Li X, Small M (2012) Neuronal avalanches of a self-organized neural network with active-neuron-dominant structure. Chaos 22: 023104. https://doi.org/10.1063/1.3701946 PMID: 22757511
13. Scarpetta S, de Candia A (2013) Neural avalanches at the critical point between replay and non-replay of spatiotemporal patterns. PLoS One 8: e64162. https://doi.org/10.1371/journal.pone.0064162 PMID: 23840301
14. Kihara AH, Tsurumaki AM, Ribeiro-do-Valle LE (2006) Effects of ambient lighting on visual discrimination, forward masking and attentional facilitation. Neurosci Lett 393: 36–39. https://doi.org/10.1016/j.neulet.2005.09.033 PMID: 16229950
15. Kinjo ER, Higa GS, Morya E, Valle AC, Kihara AH, et al. (2014) Reciprocal regulation of epileptiform neuronal oscillations and electrical synapses in the rat hippocampus. PLoS One 9: e109149. https://doi.org/10.1371/journal.pone.0109149 PMID: 25299405
16. Schmeltzer C, Kihara AH, Sokolov IM, Rudiger S (2015) Degree Correlations Optimize Neuronal Network Sensitivity to Sub-Threshold Stimuli. PLoS One 10: e0121794. https://doi.org/10.1371/journal.pone.0121794 PMID: 26115374
17. Hennig MH, Adams C, Willshaw D, Sernagor E (2009) Early-stage waves in the retinal network emerge close to a critical state transition between local and global functional connectivity. J Neurosci 29: 1077–1086. https://doi.org/10.1523/JNEUROSCI.4880-08.2009 PMID: 19176816
18. Kihara AH, Paschon V, Cardoso CM, Higa GS, Castro LM, et al. (2009) Connexin36, an essential element in the rod pathway, is highly expressed in the essentially rodless retina of Gallus gallus. J Comp Neurol 512: 651–663. https://doi.org/10.1002/cne.21920 PMID: 19051319
19. Kihara AH, de Castro LM, Moriscot AS, Hamassaki DE (2006) Prolonged dark adaptation changes connexin expression in the mouse retina. J Neurosci Res 83: 1331–1341. https://doi.org/10.1002/jnr.20815 PMID: 16496335
20. Deans MR, Volgyi B, Goodenough DA, Bloomfield SA, Paul DL (2002) Connexin36 is essential for transmission of rod-mediated visual signals in the mammalian retina. Neuron 36: 703–712. PMID: 12441058
21. Kosaka T, Deans MR, Paul DL, Kosaka K (2005) Neuronal gap junctions in the mouse main olfactory bulb: morphological analyses on transgenic mice. Neuroscience 134: 757–769. https://doi.org/10.1016/j.neuroscience.2005.04.057 PMID: 15979807
22. Christie JM, Bark C, Hormuzdi SG, Helbig I, Monyer H, et al. (2005) Connexin36 mediates spike synchrony in olfactory bulb glomeruli. Neuron 46: 761–772. https://doi.org/10.1016/j.neuron.2005.04.030 PMID: 15924862
23. Lau PM, Bi GQ (2005) Synaptic mechanisms of persistent reverberatory activity in neuronal networks. Proc Natl Acad Sci U S A 102: 10333–10338. https://doi.org/10.1073/pnas.0500717102 PMID: 16006530

24. Ji D, Wilson MA (2007) Coordinated memory replay in the visual cortex and hippocampus during sleep. Nat Neurosci 10: 100–107. https://doi.org/10.1038/nn1825 PMID: 17173043

25. Luczak A, Maclean JN (2012) Default activity patterns at the neocortical microcircuit level. Front Integr Neurosci 6: 30. https://doi.org/10.3389/fnint.2012.00030 PMID: 22701405

26. Nadasdy Z, Hirase H, Czurko A, Csicsvari J, Buzsaki G (1999) Replay and time compression of recurring spike sequences in the hippocampus. J Neurosci 19: 9497–9507. PMID: 10531452

27. Girardeau G, Zugaro M (2011) Hippocampal ripples and memory consolidation. Curr Opin Neurobiol 21: 452–459. https://doi.org/10.1016/j.conb.2011.02.005 PMID: 21371881

28. Carr MF, Jadhav SP, Frank LM (2011) Hippocampal replay in the awake state: a potential substrate for memory consolidation and retrieval. Nat Neurosci 14: 147–153. https://doi.org/10.1038/nn.2732 PMID: 21270783

29. Campos JGF, Costa AA, Copelli M, Kinouchi O (2017) Correlations induced by depressing synapses in critically self-organized networks with quenched dynamics. Phys Rev E 95: 042303. https://doi.org/10.1103/PhysRevE.95.042303 PMID: 28505838

30. Rasmussen RG, Schwartz A, Chase SM (2017) Dynamic range adaptation in primary motor cortical populations. Elife 6.

31. Scarpetta S, Giacco F (2013) Associative memory of phase-coded spatiotemporal patterns in leaky Integrate and Fire networks. J Comput Neurosci 34: 319–336. https://doi.org/10.1007/s10827-012-0423-7 PMID: 23053861

32. de Arcangelis L, Herrmann HJ (2010) Learning as a phenomenon occurring in a critical state. Proc Natl Acad Sci U S A 107: 3977–3981. https://doi.org/10.1073/pnas.0912289107 PMID: 20160107

33. Bjorklund A, Dunnett SB (2007) Dopamine neuron systems in the brain: an update. Trends Neurosci 30: 194–202. https://doi.org/10.1016/j.tins.2007.03.006 PMID: 17408759

34. Stein PS (2013) Molecular, genetic, cellular, and network functions in the spinal cord and brainstem. Ann N Y Acad Sci 1279: 1–12. https://doi.org/10.1111/nyas.12083 PMID: 23530997